Defense Technical Information Center Compilation Part Notice

ADP021703

TITLE: Multispectral, Hyperspectral, and Three-Dimensional Imaging Research at the U.S. Army Research Laboratory

DISTRIBUTION: Approved for public release, distribution unlimited

This paper is part of the following report:

TITLE: Proceedings of the International Conference on International Fusion [6th]. Held in Cairns, Queensland, Australia on 8-11 July 2003. Volume 1: FUSION 2003

To order the complete compilation report, use: ADA442007

The following component part numbers comprise the compilation report:
ADP021634 thru ADP021736

Multispectral, Hyperspectral, and Three-Dimensional Imaging Research at the U.S. Army Research Laboratory

A. C. Goldberg, B. Stann, and N. Gupta
EO/IR Technology Branch
U. S. Army Research Laboratory
Adelphi, MD 20783, USA
arniecy@arl.army.mil

Abstract - *We report on the development and application of multispectral infrared imaging technology to problems of interest to the U. S. military. For tactical applications, we show the application of dual-band infrared focal plane arrays to reconnaissance, surveillance, and target acquisition. We describe the development of a new dual-band LWIR/LWIR focal plane array for detection of the disturbed soil features associated with buried land mines. We will describe the application of dual-band FPAs in the strategic defense arena by presenting dual-band MWIR/LWIR imagery of commercial launch vehicles that shows the utility of such an FPA for a sensor in a boost-phase interceptor. In addition, we describe the development of acousto-optic tunable filters (AOTF) for hyperspectral imaging in the MWIR and LWIR bands. These devices hold the promise of producing hyperspectral infrared imagers that are considerably smaller and lighter than current systems. The AOTF allows completely electronic spectral scanning for fast access to a discrete set of narrow spectral bands. We will discuss ARL's efforts in developing a novel scanerless laser radar (LADAR) system based on the frequency modulated continuous wave (FMCW) technique. This "flash" LADAR system uses a focal plane array to image the return signals from chirped pulses from a solid state laser to determine both 2D image and range information about a target. This data can then be used to construct a 3-dimensional picture of the target.*

Keywords: Infrared, Multispectral, AOTF, Hyperspectral, LADAR.

1 Introduction

The United States Army is currently engaged in a major transformation to a new Objective Force. One of the principal components of this transformation is the replacement of today's heavy main battle tanks and other fighting vehicles with a suite of lighter, highly mobile and deployable vehicles known as the Future Combat System (FCS) vehicles. To accomplish their missions, the FCS vehicles will rely on a collection of autonomous and networked sensors both on and off the vehicles. It is envisioned that these sensors will enable the crew to identify hostile targets before the enemy can detect them. An integral part of this sensor suite will be an infrared (IR) thermal imaging (TI) system for such tasks as reconnaissance, surveillance, and target acquisition (RSTA). The IR imaging system for FCS will need to have significantly enhanced capabilities over present-day 2nd generation forward looking IR (FLIR) imagers. The new sensor system will need to have significant overmatch relative to capabilities of our adversaries such that US forces can identify targets at ranges beyond those that the friendly forces can be detected by the enemy. The quantum leap in performance envisioned for these sensors will define a new generation of TI systems, the 3rd generation FLIR. One of the principal enhancements envisioned for the next generation FLIR is multispectral imaging. Over the last few years, there has been much effort put into the development of focal plane arrays (FPAs) capable of imaging in two bands of the infrared (IR) spectrum simultaneously. Some of the motivations for dual-band IR imaging are enhanced detection of targets in clutter, the ability to distinguish between targets and decoys, and remote absolute temperature measurement. These efforts have produced infrared focal plane arrays (FPAs) operating at two wavelengths in the mid-wave infrared (MWIR, 3 to 5 μm) and the long-wave infrared (LWIR, 8 to 12 μm) as well as FPAs operating in both the LWIR and MWIR. It is postulated that a dual-band IR imager with image fusion algorithms implemented in hardware, software, or both would be advantageous over single-color IR cameras (either LWIR or MWIR) because it could operate in a wider range of ambient conditions and be more effective in defeating IR countermeasures such as smoke, camouflage, and flares.

The U. S. Army Research Laboratory (ARL) has supported the development of multi-spectral IR imaging through the Federated Laboratory Advanced Sensors Consortium and, more recently, through its successor, the Advanced Sensors Collaborative Technology Alliance (CTA). As a result of these programs, ARL and its industry partners have produced dual-band MWIR/LWIR pixel-registered and simultaneously integrating focal plane arrays in both the GaAs-based quantum well infrared photodetector (QWIP) and mercury-cadmium telluride (HgCdTe or MCT) based photodiode detector technologies.

The detection and recognition of objects and backgrounds would be enhanced by the development of imagers that can detect both spectral and polarization signatures from the scene. Spectral features arise due to the material properties of objects (chemical composition) as a result of the emission, reflection, and absorption of light. Polarization features arise from the physical nature of the object surface (roughness) and edges that influence the polarization properties of the reflected, scattered, or emitted light. In general, man-made objects have more defined polarization signatures than natural objects such as soil and vegetation that generally have irregular shapes. These natural objects, often make up background scenarios of interest in many applications. Besides their shapes, objects and backgrounds have unique spectral signature information that can be used for discrimination and identification. Hyperspectral imaging can acquire images with narrow spectral bands and take advantage of the characteristic spectral signatures of different materials making up objects and backgrounds. By combining both polarization and hyperspectral detection capabilities in one single imager, we can perform much better object detection and identification than by using either polarization or hyperspectral capability alone.

At ARL, we are developing small, vibration-insensitive, robust, remotely controlled, and programmable hyperspectral imagers over the full optical spectrum to carry out Army-specific day/night imaging applications in the field for the 3rd Generation FLIR imagers for the FCS. Acousto-optic tunable filter (AOTF) based hyperspectral/multispectral imaging systems are ideally suited for such portable instruments due to their very fast operation (microseconds). Such imagers require a minimum amount of data processing because they can collect data at only select wavelengths of interest and the selected wavelengths can be changed according to the needs of the scene of interest. This agility in data collection is quite critical for military applications because it greatly reduces the data processing requirements associated with hyperspectral data collection and utilization. An AOTF is also a polarization sensitive device because the diffracted beams from it are orthogonally polarized. By combining it with another polarizing device, a polarizer/analyzer system can be developed. Here we describe our program, the development of a compact, lightweight, agile, field-portable, visible-to-near-IR (VNIR) AOTF-based spectropolarimetric imager, and present some of the field data collected using this imager. This imager uses a tellurium dioxide (TeO_2) noncollinear AOTF as an agile spectral selection element and a nematic liquid-crystal variable retardation (LCVR) plate as a tunable polarization selection device with an off-the-shelf charge coupled device (CCD) camera and optics. The spectral range of operation is from 400 to 900 nm with a 10-nm spectral resolution at 600 nm. Each spectral image is acquired with two retardation values corresponding to the horizontal and vertical incident polarizations. The operation of the imager and image acquisition is computer controlled. Image analysis is carried out using the commercial hyperspectral software package ENVI 3.4. Similar imagers are being developed to cover the ultraviolet (UV) spectral range from 220 to 480 nm and IR spectral range from 1 to 10 μm.

In addition, ARL is researching scannerless laser radar (LADAR) systems for smart munition and reconnaissance applications. These LADARs are incoherent designs that are based on a unique frequency-modulation/continuous wave (FM/CW) ranging architecture.[1] In the early stages of the program, ARL constructed a single pixel breadboard ladar that could be scanned to collect three-dimensional images of targets. This breadboard demonstrated that low power laser diodes (less than 100 mW) could be modulated to 1.2 GHz with a high depth of modulation, and that an optically incoherent ladar built on FM/CW radar principles was a promising concept. Additionally it was shown that high-resolution three-dimensional ladar data when displayed on a stereo workstation monitor substantially helped a viewer interpret a complex or cluttered scene and locate military vehicles. This fact solidified interest in pursuing LADAR as a sensor for smart munition and reconnaissance applications. ARL's first scannerless design was built and tested in 1998.[2] This design was built around a two-watt diode laser as a transmitter and an image intensifier tube as a demodulating receiver. Although the LADAR did not perform as well as expected because of shortcomings in the system circuitry, it demonstrated that direct three-dimensional imaging was possible using FM/CW ranging principles. This success encouraged a redirection of the program to develop the components and devices necessary to build a compact, solid-state breadboard LADAR; these components include eye-safe laser illuminators, "self-mixing" FPAs, and high-speed signal processors.

2 Multispectral IR Imaging

ARL has supported the development of multi-spectral IR imaging through the Federated Laboratory Advanced Sensors Consortium and, more recently, through its successor, the Advanced Sensors Collaborative Technology Alliance (CTA). As a result of these programs, ARL and its industry partners have produced dual-band MWIR/LWIR pixel-registered and simultaneously integrating focal plane arrays in both the GaAs-based quantum well infrared photodetector (QWIP) and mercury-cadmium telluride (HgCdTe or MCT) based photodiode detector technologies. The details of the fabrication and performance measurements of these FPAs has been reported elsewhere.[3]

2.1 Tactical Vehicles

Measurements were taken in the field using both QWIP and MCT dual-band FPAs. Targets of military interest such as tactical vehicles were imaged hourly over a 72-hour period. Figure 1 shows imagery taken of an M60 tank during daylight and at night. The effects of the diurnal cycle on the target and background are substantial. There were times when the targets virtually disappeared in the MWIR band.

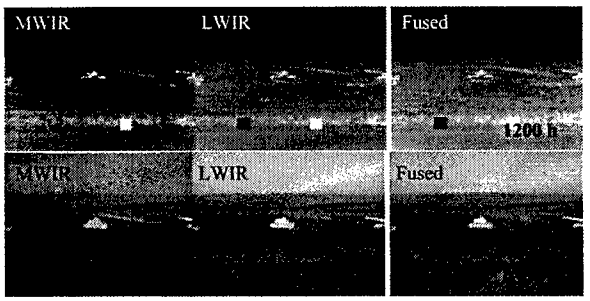

Figure 1. MWIR and LWIR IR images of an M60 tank acquired in mid-afternoon (top) and late at night (bottom) with the dual-band IR camera and the color fusion of those images

2.2 Land Mines

Figure 2 shows imagery collected with a newly developed dual-band LWIR FPA on buried land mines. This new FPA shows the potential of dual-band IR imaging for remote detection of the disturbed soil associated with buried mines. Disturbed soil has been shown to have enhanced emissivity in the 8.5 μm to 9.5 μm wavelength band while its emissivity at wavelengths greater than 10 μm is basically unchanged by disturbances. This FPA attempts to take advantage of this phenomenon (due to restrahlen effect in the mineral quartz) by the use of pixel-registered "blue" and "red" detectors which are sensitive to 9.3 μm and 10.4 μm, respectively. The image from the longer wavelength "red" pixels are used as a background from which the "blue" image data may be subtracted to enhance the visibility of the disturbed soil features. Figure 2 shows a portion of a road that had anti-tank mines buried under it. The disturbed soil above the mines shows up clearly as bright areas in the blue image but are of much lower contrast in the red image. The bottom image in Figure 2 is a fused subtraction of the red and blue images (red – blue). Positive values are assigned to shades of red and negative values are assigned to shades of blue. As expected, the subtraction enhances the visibility of the targets. The blue areas indicate the presence of disturbed soil associated with buried mines.

2.3 Ballistic Missiles

The IR signatures of rocket vehicles and their plumes in boost phase are of great importance to the Missile Defense Agency (MDA). It is well known that the rocket plume presents a large MWIR signal. However, for boost-phase interception of intercontinental ballistic missiles (ICBMs) it is necessary to image the hardbody of the missile itself, which has its strongest emission in the LWIR part of the spectrum. Image data has been collected with the dual-band QWIP FPA of commercial launch vehicles such as the new Atlas 5 Evolved Expendable Launch Vehicle (EELV). These rockets are similar in many ways to strategic ICBM threats. The utility of a dual-band IR camera for imaging the rocket plume and missile body simultaneously is shown in Figure 3. This is a very important capability for a boost-phase intercept scenario. Figure 3 shows an image taken during the inaugural flight of the Atlas 5 on August 21, 2002. This particular image was taken about 2 minutes after liftoff when the rocket was at a range of 35 km and an altitude of 24 km. The top image is displayed using the full dynamic range of the image data (14 bits) and shows the structure of the plume in the MWIR and LWIR bands.

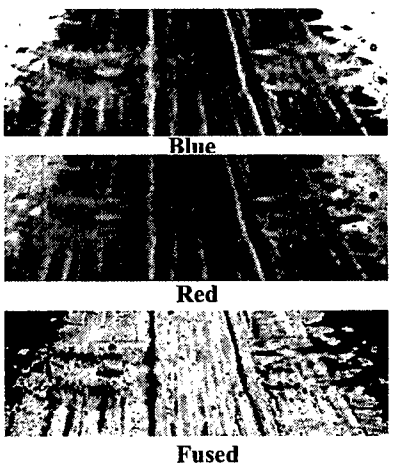

Figure 2. Simultaneous composite images of buried land mines from the blue (top), and red (center) parts of the dual-band QWIP FPA. The image at the bottom is the fused subtraction of the red and blue images.

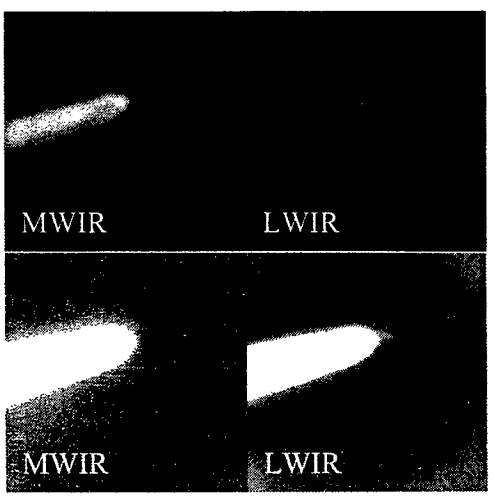

Figure 3. Dual-band IR images of the Atlas 5 launch of August 21, 2002.

The bottom image in Figure 3 is enhanced to show the lower 7 bits of the image data. In the lower image the plume signature saturates in both bands but the LWIR image clearly shows the rocket vehicle (which is not seen at all in the MWIR image).

3 AOTF Hyperspectral Imager

In an AOTF, a radio frequency (RF) signal is applied to a piezoelectric transducer that is attached to a birefringent crystal to produce an ultrasonic wave that travels through the crystal. This sets up a moving diffraction grating in the crystal. An acoustic absorber absorbs the sound wave after it traverses the crystal. When light is incident on such a crystal, it is diffracted by the traveling acoustic wave, and produces a diffracted beam with a Doppler shift for a particular wavelength based on the phase-matching condition. The diffracted wavelength can be tuned by changing the applied RF. The diffracted wavelength is inversely proportional to the applied RF.[4],[5] Figure 4 shows the diffraction of white light by a noncollinear AOTF. As shown in Figure 4, the two diffracted beams are orthogonally polarized and in our imager we use only one diffracted beam; the other two beams are blocked. Previous work has shown the utility of AOTF based spectropolarimetric imaging.[6],[7]

3.1 VNIR Spectropolarimetric Imager

ARL has developed AOTF based spectropolarimetric and hyperspectral imagers (HSI) covering wavelength regions from UV to the LWIR using different birefringent acousto-optic materials.[8]. In this work, we present data from the visible-near IR (VISNIR) system operating in the wavelength range between 0.4 and 0.9 μm.

We use a commercial LCVR (Meadowlark Optics, model LRC 100) as a retardation element that is controlled by software to produce a different retardance at each wavelength such that the incident light with either 0° or 90° polarization has 0° polarization after passing through the LCVR. The optical layout of the imager is shown in Figure 5. We use two irises to define the field of view for the incident beam and to block the unwanted beams after the AOTF (refer to Figure 4) in this imager. Also, two single lenses are used in a confocal configuration, such that the light from a distant object is first imaged at the center of the AOTF crystal and then re-imaged on a commercial 640 × 480-pixel Si-CCD camera (Watec) with an objective lens. The entire optical system is packaged in a 6×8×4 in^3 box and weighs less than 5 lbs (1.52 kg). The RF power used to drive the AOTF is less than 1 W. The imaging system is completely automated. Both the rf synthesizer (Brimrose Corp., PPS driver) and the LCVR are controlled using a personal computer. RF is changed between 50 and 120 MHz to correspond to the desired optical wavelength. The CCD output is captured using a frame grabber (EPIX, PIXCI® SV4 Imaging Board) and stored on hard drive. We developed a graphical user interface for seamless operation of the imager.

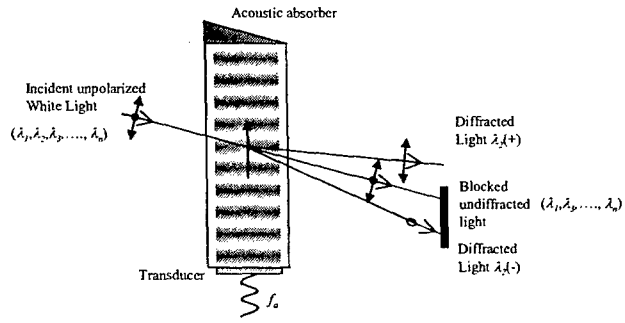

Figure 4. Diffraction of white light by a noncollinear AOTF.

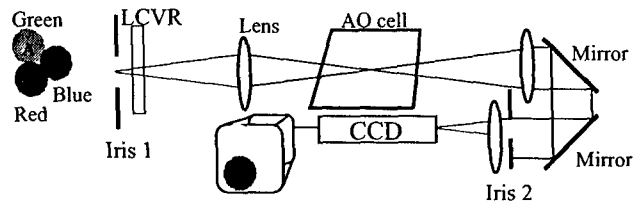

Figure 5. Layout of VNIR imager.

We have carried out a number of data collection exercises using the VNIR AOTF imager. Analyses of these data have clearly shown that manmade objects have polarimetric signatures and these signatures are affected by the viewing conditions.[9] Also, it is found that natural backgrounds like foliage do not have polarization signatures.10 Here we present three examples of the outdoor data collected by the VNIR imager. We have carried out detailed analysis of these data, and here we include the detailed results for only the first example.

The first example is from a data collection carried out on a clear sunny day on September 13, 2001 around 3 pm. Images were collected from 400 to 800 nm with a 10 nm step. We collected each image with both horizontal and vertical polarizations. The images included here are raw images. In Figure 4 images shown are for an open top HMMWV with a white trailer in the back. These vehicles are sitting in a white asphalt top parking lot. We only show six images starting at 450nm and ending at 700 nm with both polarizations. The corresponding polarization difference images (vertical minus horizontal) are shown in Figure 5. The silhouettes of the trailer and HMMWV show up in the polarization difference images even though the S/N is quite low. The edges show up more clearly, indicating that, as expected, there is more polarization signature from the edges. There is more vertical polarization signal from the top of the trailer even though the painted surface did not appear to be smooth and shiny. Instead it was rather worn out.

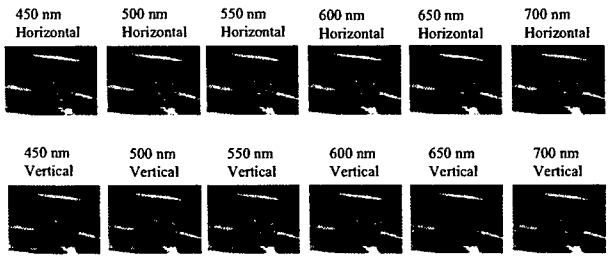

Figure 6. Spectropolarimetric images of a HMMWV and a white trailer.

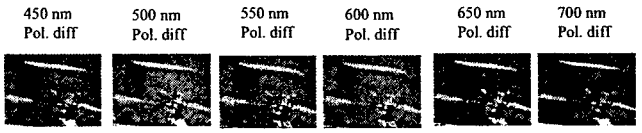

Figure 7. Polarization difference images of a HMMWV and a white trailer.

The two image cubes corresponding to the horizontal and the vertical polarization are shown in Figure 8. There are four colored squares marked on each of the two image cubes corresponding to the four points for which spectral profiles have been plotted in Figure 9.

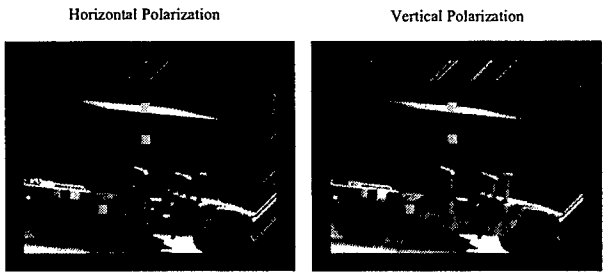

Figure 8. Image cubes for HMMWV and trailer.

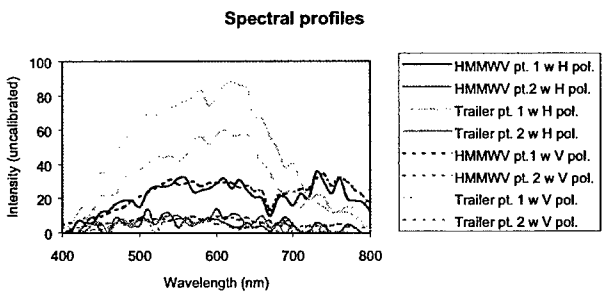

Figure 9. Spectral profiles for each of the colored squares in Figure 8.

We computed these profiles for both the image cubes. These profiles are uncalibrated and included here to show the effect of changes in both the spectral and polarimetric signatures of various pixels in the image. Each profile is an average of 5×5 pixels for the center point of each of the colored squares.

These results clearly illustrate that both the HMMWV and the trailer exhibit spectropolarimatric signatures. The difference in spectropolarimetric signatures is largest for the highly reflecting top of the trailer and relatively small for the side of the trailer and the two painted portions on the side of the HMMWV. These results correspond to the fact that most of the paints used on the trailer and HMMWV are flat.

4 3-Dimensional LADAR Imaging

4.1 Laboratory Breadboard architecture

In the following text, we briefly describe the operating principles of the 32 × 32 pixel FPA LADAR breadboard using the block diagram shown in Figure 10. A trigger circuit initiates the generation of a chirp signal that serves as the laser modulation and local oscillator (LO) signal. This chirp signal is simply a sinusoidal waveform whose frequency linearly increases over a period T and then flies back to the original start frequency (i.e. sawtooth FM). The chirp signal for our breadboard has a start frequency of 200 MHz and a stop frequency of 800 MHz. FM/CW radar ranging theory supports a rich variety of improvisations to the basic sawtooth modulation format. However, to simplify our present work with the LADAR breadboard, we use only the pure sawtooth modulation format, which yields high range resolution with the least amount of LADAR signal processing.

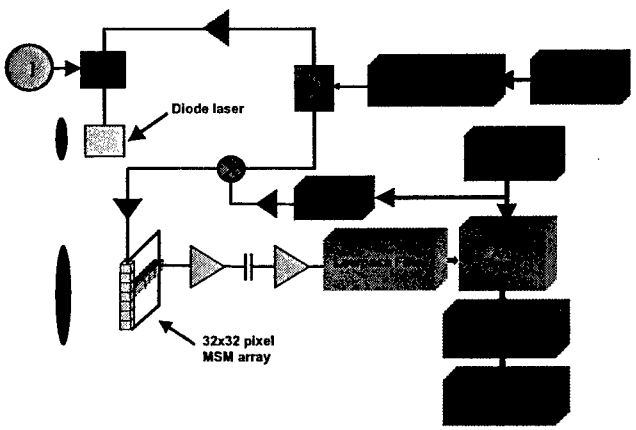

Figure 10. Laboratory ladar breadboard block diagram.

To modulate the laser illumination, the chirp signal is fed into a wideband rf power amplifier with a low output driving impedance. Output from the amplifier and a dc current are summed in a bias tee to provide a modulated current drive for a broad-area semiconductor diode laser at 808 nm with a bandwidth at least equal to the bandwidth of the chirp waveform. A high-percentage amplitude modulation of the light beam is desirable. The divergent laser beam from the semiconductor laser is collected with a collimator and focused to project a beam sufficiently wide to encompass or floodlight the target scene of interest.

A small portion of the transmitted beam is reflected from the target toward the LADAR and collected by the

receiver optics. An array of OE-mixing metal-semiconductor-metal (MSM) detectors is located at the focal plane of the receiver optics.[11],[12] When the transmitter modulation waveform (LO voltage) is applied across the OE-mixing detectors, a photocurrent response is recovered at each detector that is the product or mixing of the LO and the modulated light waveforms. With sawtooth modulation, the instantaneous transmitted and received chirp waveforms differ in frequency (by the intermediate frequency (IF)) because the round-trip light propagation time delays the received chirp waveform with respect to the LO chirp waveform. Thus, mixing of the LO and return signal in the detectors produces a sinusoidal photocurrent (IF waveform) whose frequency is proportional to range. To recover the photocurrents from the individual pixels, we employ a unique read-out based on code division multiple access (CDMA) techniques discussed in detail in another publication.[13] To implement this technique, we multiply the LO signal for each column of the array by a unique binary code. The net effect is to nearly orthogonalize the photocurrents for all pixels in a row, thus allowing all currents to be combined into a single wire that connects to a transimpedance amplifier (TIA) to the side of the detector array. The TIA converts the photocurrents into a voltage that is then sampled at the code clock rate by an analog-to-digital converter (A/D). The digital data is fed into a demultiplexer (demux) which breaks-out each pixel's photocurrent in each row; the fast Fourier transform (FFT) is taken for each of the photocurrents to map the data space into a three-dimensional image space.

4.2 32 × 32 laboratory breadboard hardware

Figure 11 shows the front view of our laboratory breadboard. The picture is centered on the fan-in/fan-out board where microstrip LO and IF signal lines are evident leading into a socket that holds a leadless chip carrier containing the MSM array. A 5 cm diameter camera lens receives the backscattered target light and focuses it onto the OE-mixing MSM detector array. In early operation of the breadboard, scene illumination was achieved with a 100 mW GaAs diode laser mounted in the "L" shaped aluminum block. More recently, a 2 W GaAs diode laser has replaced the lower power laser to allow full-field imaging. Output from the laser is collimated and directed toward a mirror that reflects the laser light toward a target in the receiver field of view (FOV). The mirror's angular position can be controlled with a pair of micrometers enabling us to steer the laser beam around the receiver's FOV, i.e. over the receiver's FPA. The receiver lens position is also adjustable to steer the FOV around the target scene and to adjust the focus.

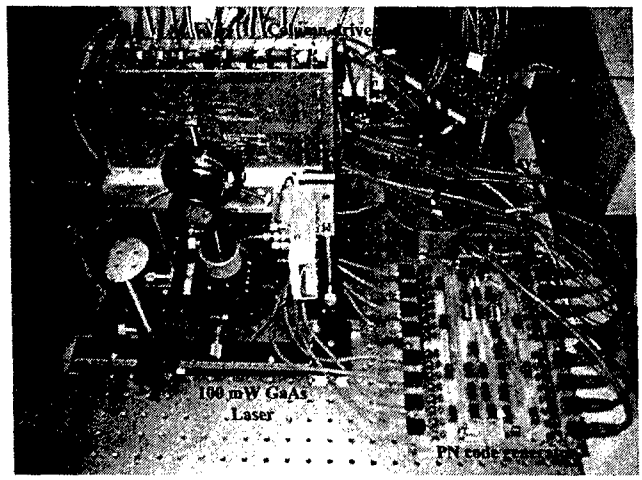

Figure 11. Front (top) view of 32 × 32 pixel laboratory breadboard,

For the receiver's FPA, we fabricated a 32 × 32 pixel interdigitated-finger MSM FPA on semi-insulating GaAs. Each detector in the array consists of 3-μm wide fingers with 5-μm wide finger spacings. The active area of each device is 60 × 60 μm2. Fabrication of the array consists of a four-step process with optional steps to either enhance or simplify the array. Initially, interdigitated Ti/Au Schottky contacts are deposited on the GaAs with the planar pattern of the metallization defined by standard photolithographic procedures and lift-off techniques. Then the whole sample is coated with silicon dioxide. This dielectric serves two purposes: First, it acts as an anti-reflection coating to enhance the MSM responsivity. And second, it forms the dielectric for bypass capacitors that are fabricated at the output of each row. After the dielectric has been deposited, windows are etched for bonding and vias are etched for crossover connections. Finally, a second layer of metal is evaporated which electrically connects the rows and columns. Following fabrication, the array is diced from the wafer, tested, epoxied, and wire bonded into a commercial leadless chip carrier.

4.3 Results of laboratory breadboard tests

The purpose of this section is to briefly discuss some basic experiments designed to measure the performance of our laboratory breadboard. In the first experiment, we determined pixel-to-pixel isolation along an individual row. The laser beam was collimated into a small spot and projected onto a poster board 10 m away. The received light was focused onto a single pixel in a row, and the data were processed in the usual manner to determine the range and amplitude for the pixel on which the light was impinging. Figure 7 shows the processed data for one row in the array where for (a) the laser beam was projected onto the leftmost pixel of the FPA. The top graph of figure 7(a) is a false color plot that graphs pixel intensity as a function of pixel row position (abscissa) and range (ordinate). The scale on the ordinate is in terms of

resolution cells that correspond to .25 m in range; here the return peaks at 40 range cells, which is equal to the range to the target (10 m). The processor also reports that the light is indeed on the leftmost pixel of the FPA. The bottom graph of figure 12(a) plots pixel intensity at the target range as a function of row position. Problems with cross-talk on the breadboard are now evident since low but not insignificant signal voltage appears in pixels that are not illuminated. This behavior is also present when the light is on other pixels as shown in figures 12(b) and 12(c).

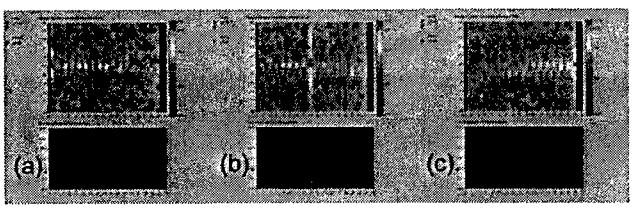

Figure 12. Pixel intensity versus range and pixel position.

The highest cross-talk levels occur at every other pixel position starting from the position where the light is directed. The LO drives are fed in alternately from the top and the bottom of the FPA; thus, adjacent drives are connected to every other FPA column. This leads us to conclude that the cross-talk is caused by capacitive coupling between adjacent microstrip lines and between the conductors internal to the FPA package. Further support for this conclusion follows from the observation that the cross-talk is quite low between the illuminated pixel and pixels in columns that are driven from the opposite side of the array. This also indicates that cross-talk between adjacent pixels internal to the FPA is low. Measurements of the S12 parameter between adjacent contacts on the FPA package is around –20 dB for most of the 200-800 MHz band; this also supports the conclusion that the cause of the cross-talk is inter-electrode capacity between adjacent microstrip lines and between FPA package conductors.

The last test of the breadboard focused on collecting a rudimentary image in the lab. To achieve this, a copy of the illumination module built for the line imaging ladar was constructed and installed in the breadboard3. By defocusing the module's collimator, it projects a .60 m square illumination field at 10 m distance from the ladar breadboard. The laser current is set to yield a light output of just under 2 W, and the modulator drive parameters are set to achieve a modulation index of approximately 80%. The original receiver lens in the breadboard was exchanged for one with a shorter focal length but equivalent aperture to enlarge the receiver FOV to about 38 cm. A poster board placed at 10 m range acted as a backstop and a 31 cm high by 31 cm wide cardboard "A" placed 2 m in front of the backstop served as a target. The lines in the target lettter "A" were 2.5 cm wide. Three views of the resulting image are shown in Figure 13. Note that the LADAR data was collected from a single, front facing viewpoint in two frames (one frame to collect data from the upper half of the FPA and a second frame to collect data from the lower half of the FPA). The images were obtained after performing the processing steps discussed previously, but only retaining the last returns above threshold in each pixel (last pulse logic). Figure 13 (a) is a three-quarters rendering looking slightly from the top down; here the "A" and the backdrop are clearly evident and displaced in distance as expected. The vertical structures on the "A" are reasonably well-formed except for some missing pixels. Examination of the data shows that these pixels were operating, but canceling effects from cross-talk in the rows caused some pixel outputs to drop below threshold. The cross bar in the "A" covers approximately 20 pixels in a row, and as a consequence creates a substantial accumulation of cross coupling components that are manifest by the image artifacts present to the side and slightly before the cross bar. The problems with cross-coupling are especially onerous in the image of the backstop where all 32 pixels in all rows intercept the illumination field, except for those pixels in the shadow of the target. Here, not only are cancellation effects evident, but also appreciable signal energy is scattered into ranges forward of the backstop position. To prevent these signals from creating a noisy image, the threshold is set relatively high causing large portions of the backdrop to disappear. Figure 13 (b) is the LADAR image viewed from above the ladar viewpoint. Figure 13 (c) is the image rotated nearly 90 degrees with respect to the LADAR viewpoint; here the displacement of the backstop and the "A" are most pronounced.

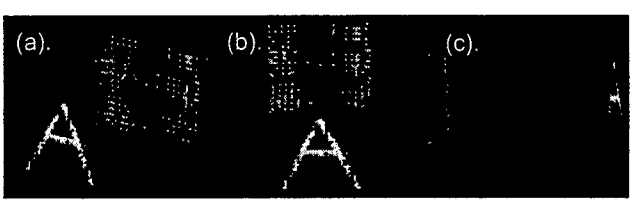

Figure 13. Breadboard ladar image, three-quarter view (a), front view (b), side view (c).

As of this date, the results with the 32 × 32 pixel breadboard show considerable promise for acceptable performance given that the cross-coupling between FPA columns can be suppressed. A reasonably well-formed range response to a target is recovered, and the noise floor is near what should be expected for the noise intrinsic to the TIA. For the future, the 32 × 32 pixel FPA will be mounted on a PC board designed to substantially reduce the capacitive coupling between LO feed lines. The feed-in/feed-out board will also be improved to reduce cross-coupling between the microstrip lines. Other work will include the construction of a new 32-channel data acquisition system with provision to adjust the synchronization of data sampling with the code and to perform over-sampling. A new code generator will be built that will enable the use of truly orthogonal code

sequences to further reduce cross-talk. Code will be written to process the data from the 32 rows and form a rudimentary display of the image on the PC. Recent success with the development of single MSM InGaAs OE-mixing detectors will be exploited to build a 32x32 InGaAs FPA for the LADAR breadboard. If successful, in the future, this FPA will be retro-fitted into the breadboard along with an Erbium fiber amplifier based illuminator for operation in the "eye safe" waveband at 1.5 μm. In addition, a signal processor based on FPGAs will be added to enable real-time data processing and image display.

5 Conclusions

We have presented ARL's capability in multispectral, hyperspectral, and 3D imaging LADAR. The dual-band IR detector arrays developed by ARL in conjunction with our industrial partners under the Federated Laboratory and Collaborative Technology Alliance programs have been used to collect data on targets of great interest to the U.S. military. The MCT dual-band IR camera was used to acquire data on ground vehicle targets over an entire diurnal cycle. A new dual-band LWIR/LWIR FPA was developed for mine detection and successfully detected recently buried mines. Finally, the IR signatures of the plumes and hardbody of a rocket similar to an ICBM were measured with a QWIP MWIR/LWIR FPA. These demonstrations show the usefulness of dual-band IR imagery for military. In addition, the fusion of the component images enhances the visibility of targets.

New lightweight and compact hyperspectral imagers have been developed using AOTFs. These imagers have the advantage of not only gathering spectral information about a target but they are able to obtain polarimetric data as well. We are designing and fabricating AOTF imagers that can work in the MWIR and LWIR spectral regions. These systems will have considerable advantage in weight and power considerations over existing hyperspectral imagers.

Finally, we presented our scanerless LADAR system based on FM/CW radar technique. We have shown the utility of this technique in providing high-resolution 3-dimensional images of targets without the need of a scanner. We are currently engaged in research aimed at combining this LADAR system with a passive IR FPA in a single sensor using a common ROIC and optics. The QWIP IR detector structure lends itself well to this task because of its inherently large bandwidth (>50 GHz) and the fact that both the LADAR receiver detectors and the passive IR detectors can be made using the same III-V materials such as GaAs, InGaAs, and InP.

References

[1] B. L. Stann, W. C. Ruff, Z. G. Sztankay, "Intensity-modulated diode laser radar using frequency modulation/continuous wave ranging techniques," Optical Engineering Vol. 35, No. 11, pp 3270-3278, (1996).

[2] B. L. Stann et. al., "A scannerless imaging ladar using a laser diode illuminator and FM/CW radar principles", presented at SPIE AeroSense, 6-9 April 1999; Proc SPIE Laser Radar Technology and Applications IV, Vol. 3707, (1999).

[3] A. C. Goldberg, et al, Optical Engineering, January 2003.

[4] N. Gupta, "Acousto-Optic Tunable Filters," Opt. Photon. News 8, 23–27 (1997).

[5] M. S. Gottlieb, "Acousto-Optic Tunable Filter," in Design and Fabrication of Acousto-Optic Devices, A. P. Goutzoulis and D. R. Pape, eds., Marcel Dekker, New York, pp. 197–283 (1994).

[6] D. A. Glenar, J. J. Hillman, B. Saif, and J. Bergstralh, "Acousto-Optic Imaging Spectropolarimetry for Remote Sensing," Appl. Opt. 33, 7412–7424 (1994).

[7] M.A. Sturgeon, L. J. Cheng, P. A. Durkee, M. K. Hamilton, J. F. Huth, C. Mahoney, R. C. Olsen, G. Reyes, "Spectral and polarimetric analysis of hyperspectral data collected by an acousto-optic tunable filter system," Proc. SPIE 2231, 167–176, (1994).

[8] Neelam Gupta and Rachid Dahmani , "Tunable Infrared Hyperspectral Imagers," Proc. International Symposium on Spectral Sensing Research 2001, pp.233-236, 2001.

[9] Neelam Gupta, "Remote sensing using hyperspectral and polarization images," Proc. SPIE 4574, pp.184-192, 2001.

[10] N. Gupta, L. Denes, M. Gottlieb, D. Suhre, B. Kaminsky, and P. Metes, "Object detection using a field-portable spectropolarimetric imager," App. Opt.40, pp.6626-6632, 2001.

[11] W. C. Ruff et. al., "Self-mixing detector candidates for an FM/cw ladar architecture", presented at SPIE AeroSense, 24-28 April 2000; Proc. SPIE Laser Radar Technology and Applications V, Vol. 4035, (2000).

[12] P. Shen et. al., "Interdigitated finger semiconductor photodetector for optoelectronic mixing", presented at SPIE AeroSense, 24-28 April 2000.

[13] B. L. Stann, A. Abou-Auf, K. Aliberti, J. Dammann, M. Giza, G. Dang, G. Ovrebo, B. Redman, W. Ruff, and D. Simon, "Research progress on a focal plane array ladar system using chirped amplitude modulation", presented at SPIE AeroSense, 21-25 April 2003; Proc SPIE Laser Radar Technology and Applications VIII, Vol. 3707, (2003).